JACS
JOURNAL OF THE AMERICAN CHEMICAL SOCIETY

Communication

pubs.acs.org/JACS

Unique Electronic and Structural Effects in Vanadia/Ceria-Catalyzed Reactions

Xin-Ping Wu and Xue-Qing Gong*

Key Laboratory for Advanced Materials, Centre for Computational Chemistry, and Research Institute of Industrial Catalysis, East China University of Science and Technology, Shanghai 200237, People's Republic of China

Supporting Information

ABSTRACT: Vanadia/ceria supported catalysts exhibit ultrahigh catalytic activities in oxidative dehydrogenation (ODH) reactions. Here, we performed systematic density functional theory calculations to illustrate the underlying mechanisms. It is found that unique electronic and structural effects are both crucial in the catalytic processes. Calculations of the catalytic performance of different oxygen species in oxidation of methanol to formaldehyde suggested that the oxygen of the interface V−O−Ce group is catalytically more active, especially when H adsorption energy is small, indicating the strong structural effect in the vanadia/ceria supported catalyst. In addition, new empty localized states of O 2p generated in a ceria-supported system through depositing VO_3- and VO_4-type monomeric vanadia species are determined to participate in the whole ODH reaction processes and help to reduce the barriers at various steps.

Catalysts based on supported vanadium oxide exhibit remarkable activity in selective oxidative dehydrogenation (ODH) reactions.[1−3] As compared with irreducible oxides, like silica or alumina, ceria-supported vanadia (vanadia/ceria) has been found to be particularly active.[1−3] To understand the underlying mechanism of vanadia/ceria-catalyzed ODH reactions regarding the active sites and the reaction pathways, many studies focused on the atomic structures, surface activity, and their correlations have been widely conducted.[2−8] It has been shown that strong interactions exist between monomeric vanadia clusters and the ceria support, leading to the facile domination of vanadia monomers on ceria at low vanadia loadings.[4] Temperature programmed desorption (TPD) experiments also revealed that vanadia monomers are more active for oxidation of methanol to formaldehyde compared with other oligomers on ceria support.[3]

The atomic structures of the prototype $CeO_2(111)$-supported monomeric vanadia species have been extensively studied by different groups,[5,6] and one specific VO_2 species (Figure S1) was proposed to be the active species to account for the remarkably high activity of vanadia/ceria.[3,7,8] It has been found to give high stability in the temperature range of 190−425 K at low oxygen pressure ($p = 10^{-9}$ atm)[6] and enhanced H adsorption and O vacancy formation capabilities.[3,7] Very recently, we found through systematic density functional theory (DFT) study that one new VO_2 species (Figure 1) with the structure rather different to the early one (Figure S1) is energetically more favorable to occur.[9] It should also be noted that for ODH over CeO_2-supported vanadia, the catalyst is employed in an O_2-rich environment,[2,10] and the reactions follow the Mars−van Krevelen (MvK) mechanism,[11] in which oxygen species of the catalyst actually participate in the oxidation processes. However, the catalytically active oxygen species for ceria-supported VO_x, such as the O of the VO_x, at the VO_x−ceria interface and the ceria support (Figure 2), and their relative contributions to ODH activities have not been well understood yet. Therefore, the identification of the activities of different surface oxygen species at such supported catalysts and corresponding origin of the unique activity are highly desirable. In this work, by performing DFT calculations using the PBE functional and with Hubbard U

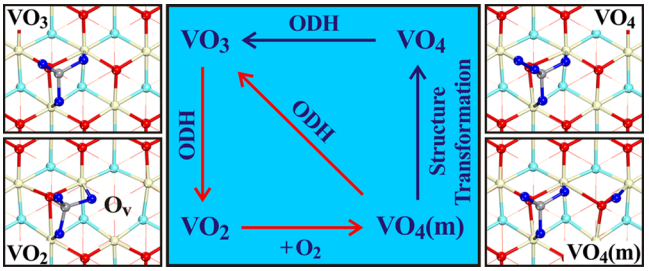

Figure 1. Structure evolution of VO_x species in ODH processes. Calculated structures of selected VO_x species are also shown. Ce atoms are in ivory, V in gray and O above the $CeO_2(111)$ surface in deep blue. O atoms of top- and subsurface are in red and cyan, respectively. Oxygen vacancy is marked with "O_v". These notations are used throughout the paper. Ce^{3+} pattern of VO_2 is shown in Figure S2.

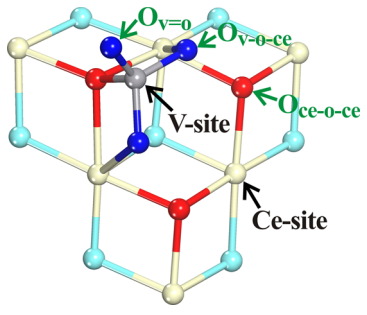

Figure 2. Different oxygen species and methanol adsorption sites. The figure is based on the VO_3 species which has common structural features with other VO_x species.

Received: July 29, 2015
Published: October 6, 2015

DOI: 10.1021/jacs.5b07939
J. Am. Chem. Soc. 2015, 137, 13228−13231

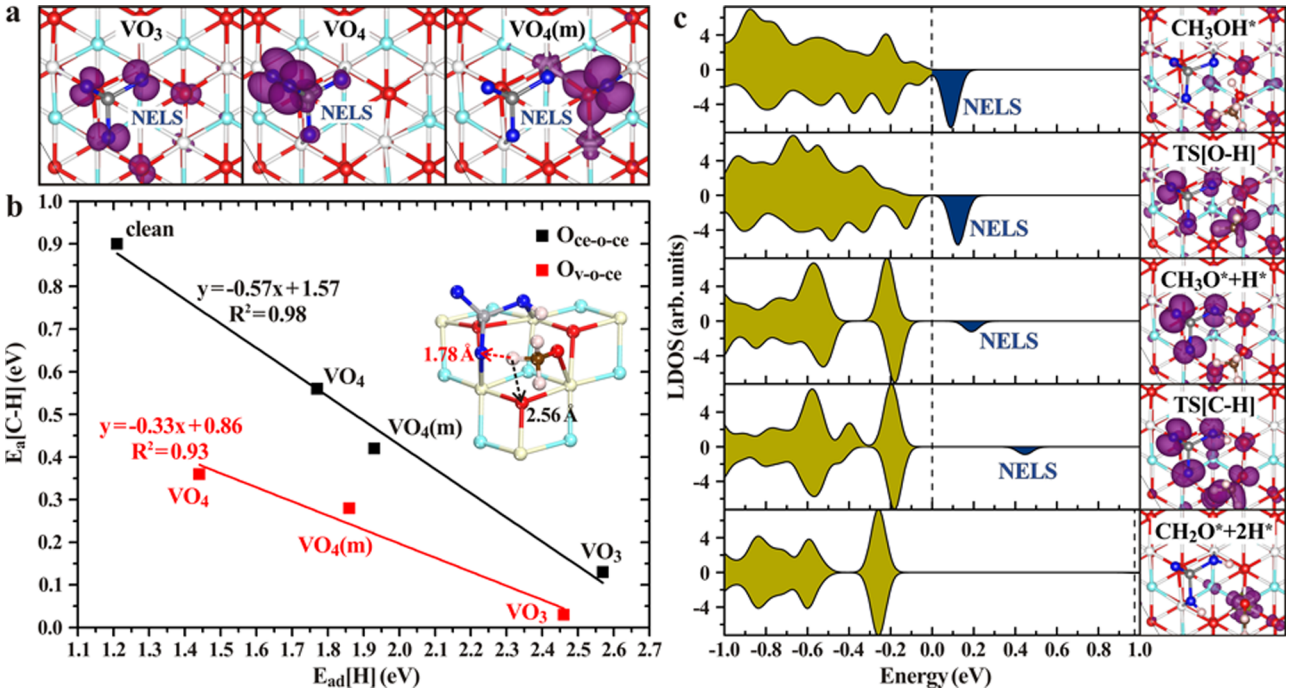

Figure 3. (a) LUMO distributions of VO_3, VO_4, and VO_4(m). Isosurface (purple) levels were set at 0.004 $Å^{-3}$. (b) Correlations for H adsorption energy and the barrier of rate-limiting C−H breaking step through $O_{ce-o-ce}$ or O_{v-o-ce} route. Inset: C−H bond breaking scheme (at VO_3). C and H atoms are in brown and pink, respectively. (c) Calculated LDOS and HOMO distributions for the states along H abstraction ($CH_3OH^* \rightarrow CH_3O^* + H^* \rightarrow CH_2O^* + 2H^*$) through O_{v-o-ce} route at VO_3. The LDOSs belong to five oxygen atoms constituting the NELS at VO_3. The occupied states and the empty states of the LDOSs were filled in yellow and dark blue, respectively. Fermi levels were indicated by the dashed lines. TS[O−H] and TS[C−H] are the transition states of O−H and C−H breaking steps, respectively. Isosurface (purple) levels of HOMO distributions were set at 0.002 $Å^{-3}$. Orbital distribution images in (a) and (c) were obtained by VESTA visualization software.[15]

(DFT+U) and Grimme's dispersion (DFT-D)[12] corrections (see Supporting Information for details),[12,13] we determined that deposition of VO_3 and VO_4 clusters on the ceria surface modifies the electronic structure of ceria, which can increase the activities of oxygen species in ODH reactions significantly. In addition, structural effect was also found to be crucial to the ODH activity: O at the V−O−Ce interface have extraordinary ability to break the C−H bond of adsorbed CH_3O.

The atomic structures of supported VO_x species have been made clear in recent years with the contributions of DFT calculations.[5,6,9] The identified most stable configurations of VO_x with given compositions (x = 2−4, labeled as VO_2, VO_3, and VO_4) are illustrated in Figure 1. The vanadium of all these species is in the highest oxidation state of +5. The calculated phase diagram at oxygen pressure of 0.21 atm (Figure S3) shows that VO_4 is the most stable species below 520 K, while VO_2 is the most stable one within higher temperature range of 520−950 K. At ∼520 K, these three different species were found to be closely competitive in stability. Therefore, we can propose a possible structural evolution pathway for these species in reactions following MvK mechanism (Figure 1). It can start from one stable species as indicated in the phase diagram (Figure S3), e.g., VO_4, followed by the removal of oxygen species, and their replenishment as surface oxygen is consumed for the elimination of abstracted H through H_2O formation and desorption and O_2 adsorption. Therefore, the whole reaction network may contain ODH and O_2 adsorption steps as well as structural evolution steps for the catalyst involving the change of its composition and configuration. Our calculations showed that O_2 can be readily adsorbed at the surface oxygen vacancy (O_v) beside VO_2, giving rise to the metastable VO_4-type species, i.e., VO_4(m), with adsorption energy of 0.68 eV. However, the VO_4(m) species is actually very difficult to evolve to VO_4 (Figure S4). Therefore, it may react with adsorbates, and the optimal redox couple in ODH reactions should be VO_3/VO_4(m), and VO_2 becomes the product of further reaction of VO_3 and precursor for recovery of VO_4(m) (red arrows in Figure 1).

It is widely recognized that H adsorption plays a decisive role in H abstraction processes of ODH reactions.[2,3] Specifically, strong H adsorption can stabilize the reaction state after H abstraction and thus lower the corresponding abstraction barrier according to the so-called Brønsted−Evans−Polanyi relation.[14] Our calculations of the H adsorption at various VO_x species (Figure S5) showed that H adsorption is quite strong at VO_3, VO_4, and VO_4(m) with the highest calculated adsorption energies of 2.57, 1.77, and 1.93 eV, respectively, while the H adsorption energies at other VO_x (x = 1−2) species and the clean CeO_2(111) surface are much smaller (<1.50 eV). Intriguingly, from calculated electronic structures, we found that for the supported systems containing VO_3 and VO_4 clusters, the lowest unoccupied molecular orbitals (LUMO) are distributed at several surface oxygen species (Figure 3a), while for the systems with other VO_x (x = 1−2) and the clean CeO_2(111), they mainly consist of Ce 4f states (Figure S6). This is clearly due to the fact that the oxygen of VO_3- and VO_4-type species fail to capture enough electrons from the vanadium which has five valence electrons only. It is also clearly shown from calculations that these unoccupied states of oxygen species are located below the unoccupied 4f states in energy. These results then elucidate that deposition of VO_3 and VO_4 clusters on the ceria surface creates new empty localized states (NELS) of O 2p in electronic structures. Such NELS are obviously more powerful in capturing

DOI: 10.1021/jacs.5b07939
J. Am. Chem. Soc. 2015, 137, 13228−13231

electrons compared with localized 4f states of surface Ce. Therefore, the catalytic activities of ceria can be dramatically attuned. In other words, for surface reduction processes, such as H adsorption, the NELS contributes a lot to the surface activity by increasing the relative stability of the final state. Accordingly, the VO_3- and VO_4-type supported species have strong capacities for H adsorption. Note that these species show some differences in H adsorption capacity though they all contain NELS. It is largely because of the fact that the NELS (LUMO) of the two VO_4-type species (VO_4 and VO_4(m)) were the antibonding orbitals (π^*_{2p}) of the adsorbed O_2 species with calculated Bader charges of around −0.6 e, i.e., they can be taken as superoxide O_2^-. Accordingly, it can be seen from Table 1 that the relative

Table 1. Energy Levels (in eV) of NELS Relative to the Fermi Level and the Energy of HOMO

	VO_3	VO_4	VO_4(m)
E(NELS)-E(Fermi)	0.15	0.65	0.64
E(NELS)-E(HOMO)	0.31	0.89	0.87

energy levels (in two different forms) of the NELS of two VO_4-type species are very close to each other, with that of VO_4 being slightly higher, while they both have higher energies than that of VO_3. As the result, VO_4(m) has slightly higher H adsorption capacity than VO_4, and VO_3 has higher H adsorption capacity than two VO_4-type species. These results further suggest that different NELS can also give rise to very different chemical effects, depending on their energy levels.

Here, oxidation of methanol to formaldehyde was taken as the prototype ODH reaction to further illustrate the unique activities of VO_x species. It involves the following H abstraction and H_2O formation processes (eqs 1−3, * indicates adsorbed state). Among them, eq 2 with C−H breaking was widely regarded as the rate-limiting step.[16]

$$CH_3OH^* \rightarrow CH_3O^* + H^* \quad (1)$$

$$CH_3O^* \rightarrow CH_2O^* + H^* \quad (2)$$

$$2H^* \rightarrow H_2O^* + O_v \quad (3)$$

For the systems with NELS (VO_3, VO_4, and VO_4(m)), methanol can adsorb on the surface with its oxygen binding to V or Ce (Figures 2 and S7). Calculations with van der Waals interaction correction showed that Ce-sites of these three structures give methanol adsorption energies of ∼1 eV, while the methanol adsorption energies are below 0.5 eV at V-sites (Figure S7). We then calculated the reactions starting with the methanol adsorption at Ce-sites of these species. Right after methanol adsorption at surface Ce, the CH_3O−H dissociation can readily occur with nearly no barrier (Figures S8−10). Then, as it can be seen from Figure 3b (inset), two different oxygen species can participate in the rate-limiting C−H breaking step, i.e., $O_{ce-o-ce}$ and O_{v-o-ce} (Figure 2). The calculated reaction barriers and energies of this key step through $O_{ce-o-ce}$ and O_{v-o-ce} routes are summarized in Table 2 (see Figures S8−10 for the total energy diagrams involving all elementary steps). As one can see, the reaction is strongly exothermic (>1 eV) for these two cases. Interestingly, we found a linear relationship between H adsorption energy and the barrier of this rate-limiting C−H breaking step for both $O_{ce-o-ce}$ and O_{v-o-ce} routes at different VO_x species (R^2 = 0.98 and 0.93, respectively). Moreover, the corresponding results at clean CeO_2(111) (E_a[C−H] = 0.90 eV

Table 2. Calculated Reaction Barriers (E_a[C−H]) and Energies (ΔE) of the Rate-Limiting C−H Breaking Step ($CH_3O^* \rightarrow CH_2O^* + H^*$) through $O_{ce-o-ce}$ and O_{v-o-ce} Routes[a]

		VO_3	VO_4	VO_4(m)
$O_{ce-o-ce}$ route	E_a[C−H]	0.13	0.56	0.42
	ΔE	−1.80	−1.45	−1.76
O_{v-o-ce} route	E_a[C−H]	0.03	0.36	0.28
	ΔE	−1.59	−1.20	−1.41

[a]Energies in eV.

via the $O_{ce-o-ce}$ route, see details in Figure S11) are also illustrated in Figure 3b and fit well with the correlation. The determined trend that the C−H bond breaking barriers decrease with the increase of H adsorption strength further supports the reliability to choose H adsorption energy as a descriptor for catalytic ODH activities. In addition, it also reflects the unique role of the NELS in attuning the activities of surface oxygen species.

It is also interesting to note from Figure 3b that the correlation line (in red) for O_{v-o-ce} of various supported VO_3- and VO_4-type species is located below that for $O_{ce-o-ce}$, indicating that the former oxygen species is more reactive in breaking the C−H bond of adsorbed CH_3O. In fact, from the calculated vibration modes (see Movie S1), we noticed that the C−H bond stretching occurs just along the C−O_{v-o-ce} direction, which helps the transfer of H toward O_{v-o-ce}. Moreover, the rather short distance between O_{v-o-ce} and H (Table S1 and inset of Figure 3b) is also beneficial to reducing the barrier of C−H bond breaking. By contrast, for C−H bond breaking via the $O_{ce-o-ce}$ route, the bond needs to be extended and rotated to point the H toward the $O_{ce-o-ce}$ to reach the transition state, which results in the relatively high barrier for this route. In addition, the different slopes of two correlation lines (−0.57 vs −0.33) further indicate that stronger structural effect exists when H adsorption energy is smaller. In general, the correlations provide a facile way for evaluation of the barriers for the rate-limiting C−H breaking step. Furthermore, it can be seen from Figure 3b that the barriers of the rate-limiting C−H bond breaking step at O_{v-o-ce} of the VO_3- and VO_4-type species are quite low (<0.4 eV). In particular, it is almost a barrierless process at VO_3, which has the highest H adsorption energy as well. Detailed calculations for the VO_2 are reported in Figures S12−13 and further confirm that O_2 adsorption occurs at VO_2 (Figure 1). These results suggest that the NELS is actually crucial to the activities of oxygen species, and VO_3- and VO_4-type species are indeed the active species of VO_x. It also reveals the key characteristics of the supported vanadia catalysts for the efficient utilization of the metastable but highly active species in catalytic reactions.

To further understand the NELS induced superior ODH activity of the VO_x species, we then studied the electronic structure evolution in reaction. Specifically, we calculated the local density of states (LDOS) and the highest occupied molecular orbital (HOMO) distributions for the surface states during H abstraction ($CH_3OH^* \rightarrow CH_3O^* + H^* \rightarrow CH_2O^* + 2H^*$) through the O_{v-o-ce} route at VO_3 (Figure 3c). From the LDOS evolution for the five oxygen atoms constituting the NELS at VO_3, we can see that the empty state (NELS, blue area) is gradually consumed with the proceeding of the reaction. In particular, though the NELS is largely consumed after O−H breaking, it is still strong enough to reduce the energy of the transition state of the rate-limiting C−H bond breaking step.

DOI: 10.1021/jacs.5b07939
J. Am. Chem. Soc. 2015, 137, 13228−13231

This is due to the fact that the quantity of the NELS consumed by the transition state is very small, and the barrier can be still significantly reduced through such slight NELS consuming process. In addition, the fact that such characteristic NELS was not observed on dimeric and trimeric VO_x species (Figure S14) also implies that aggregation of monomeric VO_x is unfavorable to ODH activity, which is largely consistent with the TPD results.[3]

The calculated HOMO evolution shows that the orbital of the reactant overlaps with the NELS at transition states and the initial NELS are gradually occupied during reaction, again proving the participation of NELS in reaction. With the completion of the dehydrogenation, the NELS is entirely consumed, and one Ce^{3+} appears as the result of the occupation of empty 4f states by the electron from the second abstracted H (see the HOMO distribution in Figure 3c bottom). It should be noted that the empty 4f states can be largely regarded as the weak NELS as they can localize electrons and prevent the reduction of V^{5+}, implying the synergic effect of ceria with supported vanadia (Figure S15). Therefore, we can also propose that the better ODH activity of reducible supports compared with irreducible supports stems from the localized states which prefers to "hold" the electrons.

In summary, the present work shows that two species, i.e., VO_3 and VO_4(m), constitute the optimal redox couple of VO_x species in ODH reactions and the high ODH activity of vanadia/ceria is basically originated from their electronic and structural effects. Specifically, the NELS can significantly increase the capabilities of oxygen species in H adsorption, and the H adsorption energy was found to be directly related to the activity of ODH reactions. By performing the *in situ* electronic structure analyses, we directly observed the participation of NELS in reaction, confirming the unique role of NELS during catalytic processes. In addition, the structural effect is also found to be crucial to the ODH reactions, with O at the interface (O_{v-o-ce}) giving better performance than $O_{ce-o-ce}$, especially when H adsorption energy is smaller and a metastable VO_4 being catalytically more important than the thermodynamically most stable one. We believe that the proposed electronic and structural effects are crucial to understanding the mechanisms of ODH reactions on vanadia/ceria or other catalytic systems and helping design related catalyst.

■ ASSOCIATED CONTENT

Supporting Information

The Supporting Information is available free of charge on the ACS Publications website at DOI: 10.1021/jacs.5b07939.

DFT computational details, calculated structures, Ce^{3+} pattern, phase diagram, H adsorption energies, LUMO distributions, adsorption configurations of methanol, and energy profiles (PDF)

Vibration modes (AVI)

■ AUTHOR INFORMATION

Corresponding Author

*xgong@ecust.edu.cn

Notes

The authors declare no competing financial interest.

■ ACKNOWLEDGMENTS

We are grateful for financial support from the National Natural Science Foundation of China (21421004, 21322307), "Shu Guang" project of Shanghai Municipal Education Commission and Shanghai Education Development Foundation (13SG30), and the Fundamental Research Funds for the Central Universities (WD1313009). We also thank the computing time in the National Super Computing Center in Jinan.

■ REFERENCES

(1) (a) Wachs, I. E. *Catal. Today* **2005**, *100*, 79−94. (b) Dinse, A.; Frank, B.; Hess, C.; Habel, D.; Schomäcker, R. *J. Mol. Catal. A: Chem.* **2008**, *289*, 28−37. (c) Taylor, M. N.; Carley, A. F.; Davies, T. E.; Taylor, S. H. *Top. Catal.* **2009**, *52*, 1660−1668. (d) Feng, T.; Vohs, J. M. *J. Catal.* **2004**, *221*, 619−629.

(2) Liu, J.; Wu, X.-P.; Zou, S.; Dai, Y.; Xiao, L.; Gong, X.-Q.; Fan, J. *J. Phys. Chem. C* **2014**, *118*, 24950−24958.

(3) Ganduglia-Pirovano, M. V.; Popa, C.; Sauer, J.; Abbott, H.; Uhl, A.; Baron, M.; Stacchiola, D.; Bondarchuk, O.; Shaikhutdinov, S.; Freund, H.-J. *J. Am. Chem. Soc.* **2010**, *132*, 2345−2349.

(4) Baron, M.; Abbott, H.; Bondarchuk, O.; Stacchiola, D.; Uhl, A.; Shaikhutdinov, S.; Freund, H.-J.; Popa, C.; Ganduglia-Pirovano, M. V.; Sauer, J. *Angew. Chem., Int. Ed.* **2009**, *48*, 8006−8009.

(5) Shapovalov, V.; Metiu, H. *J. Phys. Chem. C* **2007**, *111*, 14179−14188.

(6) (a) Popa, C.; Ganduglia-Pirovano, M. V.; Sauer, J. *J. Phys. Chem. C* **2011**, *115*, 7399−7410. (b) Popa, C.; Ganduglia-Pirovano, M. V.; Sauer, J. *J. Phys. Chem. C* **2012**, *116*, 18572−18573.

(7) Penschke, C.; Paier, J.; Sauer, J. *J. Phys. Chem. C* **2013**, *117*, 5274−5285.

(8) Kropp, T.; Paier, J.; Sauer, J. *J. Am. Chem. Soc.* **2014**, *136*, 14616−14625.

(9) Wu, X.-P.; Liu, J.; Fan, J.; Gong, X.-Q. *RSC Adv.* **2015**, *5*, 52259−52263.

(10) (a) Beck, B.; Harth, M.; Hamilton, N. G.; Carrero, C.; Uhlrich, J. J.; Trunschke, A.; Shaikhutdinov, S.; Schubert, H.; Freund, H.-J.; Schlögl, R.; Sauer, J.; Schomäcker, R. *J. Catal.* **2012**, *296*, 120−131. (b) Wu, Z.; Schwartz, V.; Li, M.; Rondinone, A. J.; Overbury, S. H. *J. Phys. Chem. Lett.* **2012**, *3*, 1517−1522.

(11) Mars, P.; van Krevelen, D. W. *Chem. Eng. Sci.* **1954**, *3*, 41−57.

(12) Grimme, S. *J. Comput. Chem.* **2006**, *27*, 1787−1799.

(13) (a) Nolan, M.; Parker, S. C.; Watson, G. W. *Surf. Sci.* **2005**, *595*, 223−232. (b) Nolan, M.; Grigoleit, S.; Sayle, D. C.; Parker, S. C.; Watson, G. W. *Surf. Sci.* **2005**, *576*, 217−229.

(14) (a) Bligaard, T.; Nørskov, J. K.; Dahl, S.; Matthiesen, J.; Christensen, C. H.; Sehested, J. *J. Catal.* **2004**, *224*, 206−217. (b) Nørskov, J. K.; Bligaard, T.; Logadottir, A.; Bahn, S.; Hansen, L. B.; Bollinger, M.; Bengaard, H.; Hammer, B.; Sljivancanin, Z.; Mavrikakis, M.; Xu, Y.; Dahl, S.; Jacobsen, C. J. H. *J. Catal.* **2002**, *209*, 275−278. (c) Logadottir, A.; Rod, T. H.; Nørskov, J. K.; Hammer, B.; Dahl, S.; Jacobsen, C. J. H. *J. Catal.* **2001**, *197*, 229−231.

(15) Momma, K.; Izumi, F. *J. Appl. Crystallogr.* **2011**, *44*, 1272−1276.

(16) (a) Burcham, L. J.; Badlani, M.; Wachs, I. E. *J. Catal.* **2001**, *203*, 104−121. (b) Wang, Q.; Madix, R. J. *Surf. Sci.* **2002**, *496*, 51−63. (c) Wong, G. S.; Concepcion, M. R.; Vohs, J. M. *J. Phys. Chem. B* **2002**, *106*, 6451−6455. (d) Döbler, J.; Pritzsche, M.; Sauer, J. *J. Am. Chem. Soc.* **2005**, *127*, 10861−10868.

DOI: 10.1021/jacs.5b07939
J. Am. Chem. Soc. 2015, 137, 13228−13231